Eur. Phys. J. C (2025) 85:1285
https://doi.org/10.1140/epjc/s10052-025-15034-8

THE EUROPEAN PHYSICAL JOURNAL C

Regular Article - Theoretical Physics

Decoupling of anisotropic wormholes via MGD in the presence of dark matter haloes

Othman Abdullah Almatroud[1,a], **M. Rizwan**[2,b], **Mohammad Alshammari**[1,c], **M. Z. Bhatti**[2,3,d], **Saleh Alshammari**[1,e], **Z. Yousaf**[2,f]

[1] Department of Mathematics, College of Science, University of Ha'il, Ha'il 2440, Saudi Arabia
[2] Institute of Mathematics, University of the Punjab, Lahore 54590, Pakistan
[3] Research Center of Astrophysics and Cosmology, Khazar University, 41 Mehseti Street, 1096 Baku, Azerbaijan

Received: 15 September 2025 / Accepted: 31 October 2025

Abstract In this manuscript, we investigate the existence of wormhole configurations bounded by fuzzy dark matter halos within the context of the minimal geometric deformation approach to gravitational decoupling. Applying this formalism, we geometrically deform the classical Morris–Thorne wormhole solution and add an extra gravitational source, denoted by $\Theta_{\mu\nu}$. The Einasto density profile for the dark matter halos is utilized to set up the temporal component of the Θ-sector. We obtain the corresponding shape function from this construction and examine its behavior to make the wormhole configuration traversable. Physical viability of the emergent spacetime is checked with a range of diagnostics. We study energy conditions and present their behavior graphically. To gain a better insight into the internal physical characteristics, we analyze the complexity factor, exoticity parameter, and anisotropy factor, which provide information about the stability and matter content of the configuration. In addition, we perform a cracking analysis to test stability in the presence of perturbations and investigate the causality condition to verify subluminal sound speeds. Our results indicate that the MGD-Einasto model facilitates the realization of wormhole configurations with controlled exotic matter content, forming a promising path for connecting dark matter halo physics to modified gravity solutions.

1 Introduction

The general relativity (GR) is the foundation of modern astrophysics and cosmology, providing a solid geometric framework that is capable of explaining gravitational waves, black holes (BHs), quasars, and even the past of the universe [1]. Its fundamental equations, Einstein's field equations (EFE), constitute the profound link between spacetime geometry and the matter-energy content of the universe [2–8]. Of the esoteric GR predictions, the most attractive are wormholes (WHs), which are hypothetical tunnels with the ability to connect distant points in the same universe or two universes. The configurations, which may also differ in their temporal nature, provide the possibility of spacetime shortcuts or even time travel. Wormholes are often broadly referred to as inter-universe or intra-universe, and are divided again according to their geometry (Euclidean or Lorentzian), stability (long-lived or short-lived), and traversability. Traversable WHs permit the transport of matter, while non-traversable WHs do not [9]. Flamm [10] was the first to propose, in 1916, the concept of a four-dimensional "road" that might link various parts of spacetime in a way different from classical geometry. He noted that the Schwarzschild solution to the EFE represents two different regions of spacetime (WHs and BHs) joined by a spacetime passage [11,12]. This concept was developed further in 1935, when Einstein and Rosen demonstrated that it is possible to connect two regions of spacetime, which are asymptotically flat, by a curvaceous structure, now referred to as the Einstein–Rosen bridge [2]. Progress was modest for almost two decades until Wheeler, in 1955, coined the word "WH" when talking about geons–solutions to the coupled Einstein–Maxwell equations [13]. These original WHs were found to be microscopic and short-

[a] e-mail: o.almatroud@uoh.edu.sa
[b] e-mail: mrizwan.math@gmail.com
[c] e-mail: dar.alshammari@uoh.edu.sa
[d] e-mail: mzaeem.math@pu.edu.pk
[e] e-mail: saleh.alshammari@uoh.edu.sa
[f] e-mail: zeeshan.math@pu.edu.pk (corresponding author)

Published online: 11 November 2025

lived. In 1973, Ellis and Bronnikov independently proposed the existence of traversable WHs [14] with the so-called Ellis drainhole as the first explicit model. Later on, Morris, Thorne, and Yurtsever extended the idea by examining the physical possibility of macroscopic traversable WHs. For further developments in various gravitational theories, readers are referred to Refs. [15–17]. Following characteristics are necessary for the Morris–Thorne (MT) WHs to be traversable and sustained [18].

i The EFE must always be followed by the WH solution

$$\Re_{\beta\eta} - \frac{1}{2}\Re g_{\beta\eta} = T_{\beta\eta}. \tag{1}$$

ii Spherically symmetric WH metric has the following generic form

$$ds^2 \equiv g_{\beta\eta}dx^{\beta}dx^{\eta} = diag\left[-A, \frac{1}{B}, r^2, r^2\sin^2\theta\right], \tag{2}$$

where $A = \exp\{2R(r)\}$ and $B = 1 - \frac{S(r)}{r}$. The redshift and shape functions are denoted by the functions R and S, respectively.

iii The traveler should experience a tolerably low tidal force from the WH. This is ensured by choosing the metric functions so that the tidal accelerations fall within tolerable bounds for humans. In practice, both the proper tidal accelerations and radial tidal accelerations need to be maintained at or below the terrestrial gravitational acceleration (about 9.8 ms^{-2}). It is feasible to create an environment in which the variations in the gravitational field during the journey are mild enough to make the WH traversable by appropriately selecting the functions R and S [19].

iv The presence of an event horizon surrounding a WH indicates an endless gravitational redshift and an infinite amount of time for a traveler to cross the horizon and enter the WH. This means that it will be impossible to escape the WH. Therefore, the absence of event horizons, which is indicated by a finite redshift function R, is required for a traversable WH.

v There must be a throat in the WH solution connecting two asymptotically flat spacetime regions.

vi The time permitted for the traveler to traverse the WH must be limited.

vii The WH throat is located at minimum distance $r = r_0$ and at WH throat

$$S(r_0) = r_0.$$

This is called a throat condition.

viii The flaring out conditions for the WH configurations is given by

$$\frac{S(r) - S'(r)}{2\,S^2(r)} > 0 \; or \; S'(r_0) < 1.$$

ix The WH geometry is implied to be asymptotically flat since the WH neck flares out. This places an additional requirement on $S(r)$ provided by

$$\lim_{r\to\infty}\frac{S(r)}{r} = 0.$$

x The condition $\frac{S(r)}{r} < 1$ for $r > r_0$ ensures that no event horizons or singularities will form in the region $r > r_0$, and it also provides the flaring out condition necessary for a traversable WH. To maintain the WH geometry's smoothness and physical feasibility, this regularity constraint is crucial.

In the past few years, the existence and physical feasibility of traversable WHs has been tested in the realm of many altered gravity models. De Falco et al. [20,21] used the general relativistic Poynting–Robertson effect as a test to differentiate between BHs and WHs and offer an observable mechanism to endorse their existence in static and spherically symmetric spacetimes. Di Grezia et al. [22] studied the role of Einstein–Cartan theory in generalizing GR by examining the influence of torsion and spin in permitting NEC violations, which are important for the stability of WHs. Stable WH configurations have been developed in various works within the context of altered theories of gravity. Naseer et al. [23] formulated models in $f(R, \mathcal{L}_m)$ gravity and in $f(R, T)$ gravity, including the Einasto density profile and complexity factor [24], both providing physically inspired matter distributions. Similarly, Malik et al. [25] studied the WH solutions in the realm of $f(R)$ gravity with scalar potentials, demonstrating that suitable field configurations can support traversable throats. Together, these investigations demonstrate the theoretical diversity of WH solutions in modified gravity and stimulate additional stability and observational analyses, which are the focus of this work. Recent work in WH physics has considered diverse extensions of gravity and realistic astrophysical environments. For example, particle dynamics and thermodynamics in bumblebee gravity were discussed by Filho et al. [26], whereas Einstein–Euler–Heisenberg gravity was used to discuss traversable WHs by Channuie et al. [27]. Observational implications have been highlighted by Jusufi and Övgün [28] and Javed et al. [29,30], who discussed gravitational lensing of wormholes through diverse mediums and modified frameworks. Thin-shell and anisotropic structures, e.g., those in Halilsoy et al. [31] and Mustafa et al. [32], showcase ways to trap exotic matter,

which conceptually aligns with the minimal geometric deformation (MGD) framework. Besides that, dynamical calculations using test particles, quasinormal modes, and condensates have been performed in nearby spacetimes [33–36]. In the current work, we advance this body of research by utilizing the MGD method to disentangle anisotropic wormhole configurations in the framework of dark matter haloes described by the Einasto profile, thus connecting exotic matter minimization with astrophysically inspired halo geometries.

The gravitational decoupling method known as MGD was created in recent years to examine the incorporation of local anisotropies into the brane-world scenario and expanded to the paradigm of star interiors in GR [37–41]. But this adaptable instrument is not limited to studying these groundbreaking ideas. The MGD technique has been used to generate several theories in this area, including Dirac stars, thermodynamic scenarios, cosmology, BH, and modified gravity [42–47]. In light of these fruitful uses, we examine the prevalence of gravitational decoupling via MGD on WH spacetime in the current paper. To illustrate how MGD functions in this situation, we have specifically distorted the well-known MT solution [18]. Intriguingly, since the significance of the new component (named as Θ-sector) offered by the MGD technique is still up for debate [48], we have solved the field equations in this study by treating this matter sector as dark fluids (dark matter or dark energy), though the normal matter sector is also included. To achieve this, we used the temporal component of the Θ^{η}_{β} source to approximate Einasto's dark matter density profile [49]. With this data, we can determine the decoupler function $H(r)$, the entire Θ^{η}_{β} tensor, and, consequently, the full energy momentum (EM) tensor of the solution, so concluding the Θ-system. This approach promotes and validates the idea that these kinds of solutions can be formed by the dark sector, which dominates our universe [50–54]. It also provides a possible interpretation of the contribution made by MGD.

The work is structured as follows: gravitational field equations along with the MGD approach about traversable WHs are covered in Sect. 2, and the determination of the shape function and evaluation of mass function is conducted in Sect. 3, which explains the use of MGD in this situation. The behavior of matter content with the help of energy conditions and EoS parameters is shown in Sect. 4. The exoticity parameter and spacetime singularity are examined in Sects. 5 and 6. Section 7 provides some stability tests. The work is finally concluded in Sect. 7.

2 General relativistic field equations and gravitational decoupling

The EFE is given by the following expression

$$G_{\beta\eta} \equiv \Re_{\beta\eta} - \frac{1}{2}\Re g_{\beta\eta} = T_{\beta\eta}. \tag{3}$$

As already mentioned, we are interested in including new elements into the EM tensor that offer novel insights on the material structure by examining the WH's interior. Thus, the simplest method to accomplish that is to write [40]

$$T_{\beta\eta} = \tilde{\mathrm{T}}_{\beta\eta} + \chi\Theta_{\beta\eta}. \tag{4}$$

where χ is a dimensionless coupling parameter, $\tilde{\mathrm{T}}_{\beta\eta}$ is the seed EM tensor, and $\Theta_{\beta\eta}$ is the novel material part, which could perhaps theoretically be a tensor, vector or scalar field. Seed EM tensor related to anisotropic matter content is given by

$$\tilde{\mathrm{T}}_{\beta\eta} = (\tilde{\mu} + \tilde{\mathcal{P}}_{\dagger})\mathrm{U}_{\beta}\mathrm{U}_{\eta} + g_{\beta\eta}\tilde{\mathcal{P}}_{\dagger} + (\tilde{\mathcal{P}}_{r} - \tilde{\mathcal{P}}_{\dagger})\mathrm{X}_{\beta}\mathrm{X}_{\eta}, \tag{5}$$

where $\tilde{\mu}$,$\tilde{\mathcal{P}}_{\dagger}$ and $\tilde{\mathcal{P}}_{r}$ stands for density, tangential and radial pressures, respectively. U^{β} represent the four velocity vector and $\mathrm{X}^{\beta} = \sqrt{1-\frac{S}{r}}\delta^{\beta}_{\eta}$ is the unit space-like vector. The following field equations are obtained by applying Eqs. (2) and (4).

$$\tilde{\mu} + \chi\Theta^{0}_{0} = \frac{S'}{r^2}, \tag{6}$$

$$\tilde{\mathcal{P}}_{r} - \chi\Theta^{1}_{1} = -\frac{S}{r^3}, \tag{7}$$

$$\tilde{\mathcal{P}}_{\dagger} - \chi\Theta^{2}_{2} = \frac{S - S'r}{2r^3}. \tag{8}$$

Here we can see that, the set of Eqs. (6)–(8) is independent of the red-shift function R. We have used $R = 0$ to ensure that we are searching for WH solutions that are traversable (vanishing or zero tidal force). Furthermore, this criterion ensures no event horizons for the WH configurations [55]. The effective or total matter variables are denoted by the amounts on the left-hand side of Eqs. (6)–(8).

$$\tilde{\mu} + \chi\Theta^{0}_{0} = \mu, \tag{9}$$

$$\tilde{\mathcal{P}}_{r} - \chi\Theta^{1}_{1} = \mathcal{P}_{r}, \tag{10}$$

$$\tilde{\mathcal{P}}_{\dagger} - \chi\Theta^{2}_{2} = \mathcal{P}_{\dagger}. \tag{11}$$

The most important thing to look at here is the effects that the Θ-sector adds to the structure. The complex set of Eqs. ((6)–(8)) is separated by applying gravitational decoupling using MGD [40]. In this case, the minimally deformed shape function $S(r)$ is given by

$$S(r) \to \tilde{S}(r) + \chi H(r), \tag{12}$$

here, we have denoted the decoupler function by $H(r)$ and original shape function by $\tilde{S}(r)$. By using Eq. (12) into Eqs. (6)–(8), we obtain the following set of equations

$$\tilde{\mu} = \frac{\tilde{S}'}{r^2}, \tag{13}$$

$$\tilde{\mathcal{P}}_r = -\frac{\tilde{S}}{r^3}, \tag{14}$$

$$\tilde{\mathcal{P}}_\dagger = \frac{\tilde{S} - \tilde{S}' r}{2r^3}. \tag{15}$$

The conservation equation corresponding to $\tilde{\mathrm{T}}_{\beta\eta}$ is given by

$$\nabla_\beta \tilde{\mathrm{T}}^\beta_\eta = 0 \Rightarrow -\tilde{\mathcal{P}}_r{}' - \frac{2(\tilde{\mathcal{P}}_r - \tilde{\mathcal{P}}_\dagger)}{r} = 0. \tag{16}$$

The equations that correspond to the Θ-sector are provided by

$$\Theta^0_0 = \frac{H'}{r^2}, \tag{17}$$

$$\Theta^1_1 = \frac{H}{r^3}, \tag{18}$$

$$\Theta^2_2 = \frac{rH' - H}{2r^3}, \tag{19}$$

and has the following expression for the conservation equation

$$\nabla_\beta \Theta^\beta_\eta = 0 \Rightarrow -\Theta^{1\prime}_1 - \frac{2(\Theta^1_1 - \Theta^2_2)}{r} = 0. \tag{20}$$

Both components, $\tilde{\mathrm{T}}_{\beta\eta}$ and $\Theta_{\beta\eta}$, are gravitationally connected since they are conserved independently. Furthermore, it should be mentioned that the conservation of $G_{\beta\eta}$ and $\tilde{\mathrm{T}}_{\beta\eta}$ leads to the conservation of the Θ-sector. Bianchi's identities suggest

$$\nabla_\beta G^\beta_\eta = 0, \tag{21}$$

Equations (3) and (4) implies

$$\nabla_\beta \tilde{\mathrm{T}}^\beta_\eta + \chi \nabla_\beta \Theta^\beta_\eta = 0. \tag{22}$$

But in the equation above, the first term on the left side is zero. Since $\tilde{\mathrm{T}}_{\beta\eta}$ denotes the conventional matter sector, the theory's underlying symmetries provide the basis for its conservation. In this instance, the theory's symmetries relate to generic coordinate transformations, or 4D spacetime diffeomorphisms. The final result, taking into account the aforementioned ideas, is $\nabla_\beta \Theta^\beta_\eta = 0$. Naturally, it is evident that $\nabla_\beta \tilde{\mathrm{T}}^\beta_\eta = 0$ when effective $T_{\beta\eta}$ is taken into account. Note that the hydrostatic equations characterizing the configuration balance are described in Eqs. (16) and (20). The absence of a term in both formulations is evident. Particularly, the term having R is missing. Indeed, this term is absent as we have taken into account $R = 0$. Nevertheless, the missing term can be recovered, and a gravitational gradient (associated with tidal force) is introduced into the system when it is not assumed that the red-shift function is constant.

3 Decoupled wormhole configurations

As previously stated, we have considered the well-established MT WH solution into consideration as a seed spacetime [18,56]. The following line element describes this WH spacetime.

$$ds^2 = diag\left[-1, \frac{1}{1 - \left(\frac{r_0}{r}\right)^{k+1}}, r^2, r^2 \sin^2\theta\right]. \tag{23}$$

Equation (23) makes it evident that $R = 0$ and $\tilde{S}(r) = r_0 \left(\frac{r_0}{r}\right)^k$ for $k > 0$. This solution satisfies all the necessary criteria to describe the WH geometry, including the flaring-out condition, and reproduces an asymptotically flat spacetime when r approaches infinity. Furthermore, as anticipated within the paradigm of GR, the matter dispersion surrounding the throat contradicts the NEC [57,58]. However, unlike in the GR settings, where a significant amount of exotic matter is required to sustain the WH configuration, it would be ideal if only a small amount of exotic matter distribution could sustain the minimally deformed solution. While it may not be possible to totally eliminate the usage of exotic matter, the MGD can serve as a regulatory mechanism. In order to verify these facts, we go deeper into the geometry and matter distribution behavior in this section.

When it comes to representing DM halos, the Einasto density profile is crucial because, compared to other popular models, like the NFW profile, it provides a more accurate representation of the radial density profiles of these halos [59–62]. A shape parameter in the Einasto density profile allows for flexible fitting to a large range of observed galaxy halo profiles. Particularly for complex configurations, this model more accurately depicts the interface between the inner and outer regions of dark matter halos [49]. Furthermore, by enabling a more thorough assessment of the gravitational lensing effects and dynamics of dark matter within

galaxies, the Einasto model gives important insights into the distribution and behavior of dark matter at many scales. It has been successfully used to extract data on spiral galaxie's core regions and surface brightness [63–65]. To close the system (18)–(19), we take into consideration a generalized form of the Einasto density profile for the dark matter halos.

$$\Theta_0^0 = \mu_0 \exp\left\{-\left(\frac{r}{h}\right)^{1/n}\right\}, \tag{24}$$

where the triplet $\{\mu_0,\ n,\ h\}$ denote the central density, Einasto index and scale length, respectively. From Eqs. (17) and (24) we get the following differential equation

$$\frac{H'}{r^2} - \mu_0 \exp\left\{-\left(\frac{r}{h}\right)^{1/n}\right\} = 0, \tag{25}$$

having solution

$$H = c - h^3\mu_0 n\Gamma\left(3n, \left(\frac{r}{h}\right)^{1/n}\right). \tag{26}$$

To maintain a portion of the WH structure outlined in Sect. 2, the decoupler function defined in Eq. (12) needs to meet $H(r_0) = 0$. This is because $\tilde{S}(r_0) = r_0$ is already met by the non-deformed shape function $\tilde{S}$. So,

$$H(r_0) = 0 \Rightarrow c = h^3\mu_0 n\Gamma\left(3n, \left(\frac{r_0}{h}\right)^{1/n}\right). \tag{27}$$

Decoupler function will become

$$H = h^3\mu_0 n\left(\Gamma\left(3n, \left(\frac{r_0}{h}\right)^{1/n}\right) - \Gamma\left(3n, \left(\frac{r}{h}\right)^{1/n}\right)\right). \tag{28}$$

Next, we have

$$S = \chi h^3\mu_0 n\left(\Gamma\left(3n, \left(\frac{r_0}{h}\right)^{1/n}\right) - \Gamma\left(3n, \left(\frac{r}{h}\right)^{1/n}\right)\right) + r_0\left(\frac{r_0}{r}\right)^k. \tag{29}$$

We have analysed the modified shape function S graphically and found that it meets with all the necessary criterion to describe the WH geometry including flaring out condition (i.e., $S'(r) < 1$), throat condition and asymptotic flatness (i.e., $\lim_{r\to\infty}\frac{S(r)}{r} = 0$). The behavior of the shape function S and the graphical analysis of these conditions is illustrated in Fig. 1. The modified space-time is then provided by

$$ds^2 = diag\left[-1, \frac{r}{\chi h^3\mu_0 n\left(\Gamma\left(3n, \left(\frac{r}{h}\right)^{1/n}\right) - \Gamma\left(3n, \left(\frac{r_0}{h}\right)^{1/n}\right)\right) - r_0\left(\frac{r_0}{r}\right)^k + r}, r^2, r^2\sin^2\theta\right]. \tag{30}$$

The flaring-out condition is given by

$$\frac{r^k\left(r_0^{k+1}(k+1)e^{\left(\frac{r}{h}\right)^{1/n}} - \chi\mu_0 r^k\left[h^3 n\left(-\Gamma\left(3n, \left(\frac{r_0}{h}\right)^{1/n}\right) + \Gamma\left(3n, \left(\frac{r}{h}\right)^{1/n}\right)\right)e^{\left(\frac{r}{h}\right)^{1/n}} + r^3\right]\right)e^{-\left(\frac{r}{h}\right)^{1/n}}}{\left(r_0^{k+1} + \chi h^3\mu_0 n r^k\left[\Gamma\left(3n, \left(\frac{r_0}{h}\right)^{1/n}\right) - \Gamma\left(3n, \left(\frac{r}{h}\right)^{1/n}\right)\right]\right)^2} > 0. \tag{31}$$

By substituting $r = r_0$ in the above equation, we get

$$\chi < \frac{(k+1)e^{\left(\frac{r_0}{h}\right)^{1/n}}}{\mu_0 r_0^2}. \tag{32}$$

By using a standard procedure [66], it is simple to obtain the mass function $\mathcal{M}$ of the WH from Eq. (6) as follows

$$4\pi\int_{r_0}^{r}(\tilde{\mu} + \chi\Theta_0^0)z^2\,dz = 4\pi\int_{r_0}^{r}S'(z)\,dz. \tag{33}$$

Consequently, the usual mass is given as

$$\tilde{\mathcal{M}} \equiv 4\pi\int_{r_0}^{r}(\tilde{\mu} + \chi\Theta_0^0)z^2\,dz. \tag{34}$$

By using throat condition (i,e., $S(r_0) = r_0$), the integral on the right side of Eq. (33) becomes

$$4\pi\int_{r_0}^{r}S'(z)\,dz = 4\pi(S(r) - r_0). \tag{35}$$

The total mass $\mathcal{M}$ of the WH is defined as

$$\mathcal{M} \equiv 4\pi\left\{r_0 + \int_{r_0}^{r}(\tilde{\mu} + \chi\Theta_0^0)z^2\,dz\right\} = 4\pi S(r), \tag{36}$$

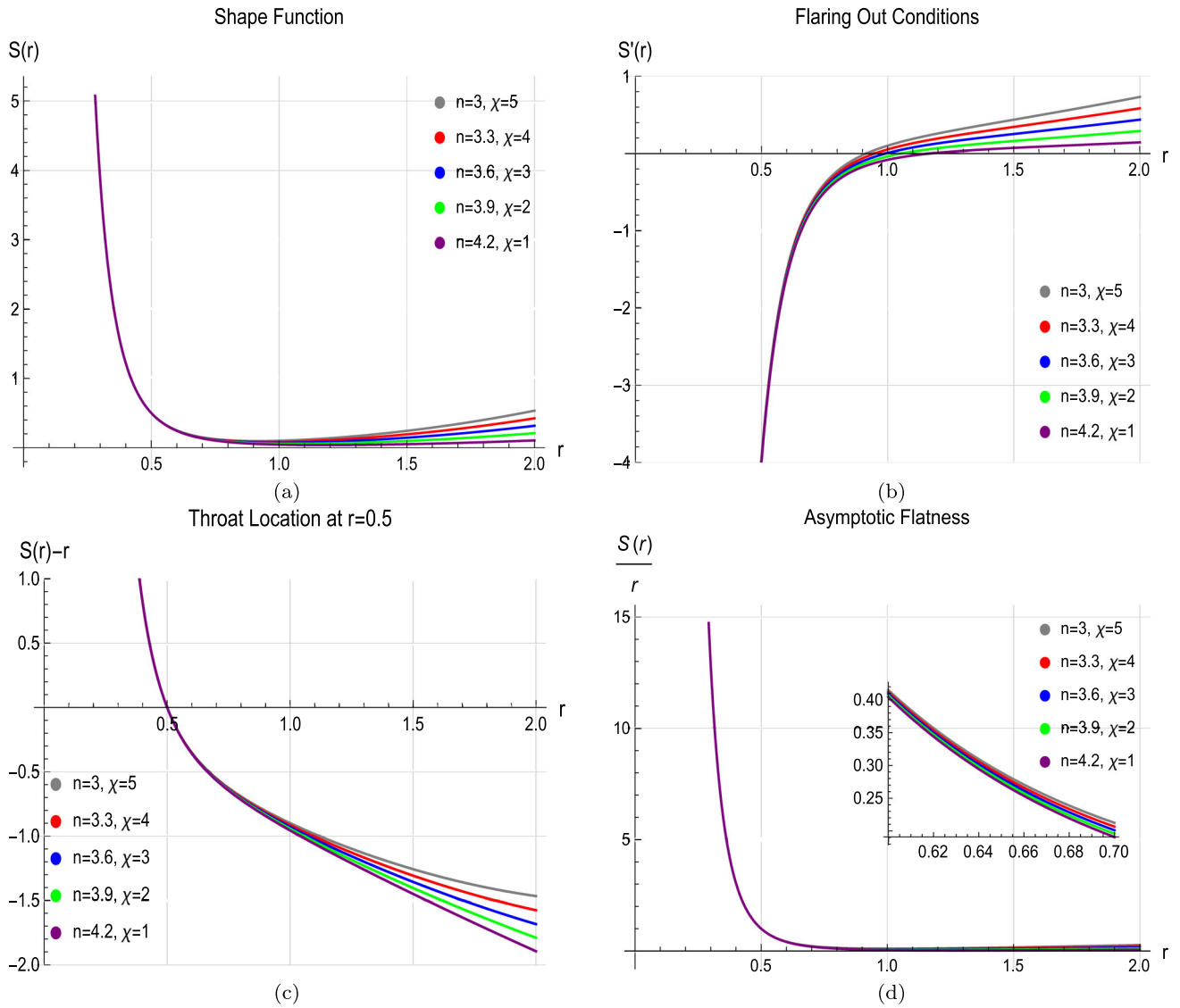

Fig. 1 Graphical depiction of wormhole conditions and shape function for $r_0 = 0.5$, k = 4, h = 2, $\mu_0 = 0.1$, and selected values of Einasto index n and dimensionless parameter χ

this implies

$$\mathcal{M} = 4\pi \left(\chi h^3 \mu_0 n \left(\Gamma \left(3n, \left(\frac{r_0}{h} \right)^{1/n} \right) - \Gamma \left(3n, \left(\frac{r}{h} \right)^{1/n} \right) \right) + r_0 \left(\frac{r_0}{r} \right)^k \right). \tag{37}$$

Since the parameters μ_0, n, h, and k all are considered to be positive in this study, the mass function $\mathcal{M}$ will be positive everywhere if and only if $\chi > 0$. By using this fact Eq. (32) will take the following form

$$0 < \chi < \frac{(k+1)e^{\left(\frac{r_0}{h}\right)^{1/n}}}{\mu_0 r_0^2}. \tag{38}$$

Behaviour of the mass function $\mathcal{M}$ is depicted in Fig. 2. In limiting case the mass function $\mathcal{M}$ is bounded i.e.,

$$\lim_{r\to\infty} \mathcal{M} = 4\pi\alpha h^3 \mu_0 n \Gamma \left(3n, \left(\frac{r_0}{h} \right)^{1/n} \right). \tag{39}$$

4 Assessment of mater distribution

Energy conditions are central in analyzing the physical viability of WH solutions, particularly in the MGD decoupling formalism. In this setup, the EM tensor is separated into a main (seed) sector and a second decoupled sector, which permits a systematic and controlled handling of the matter content. By giving a physically motivated profile, like the Einasto density distribution, to the temporal part of the addi-

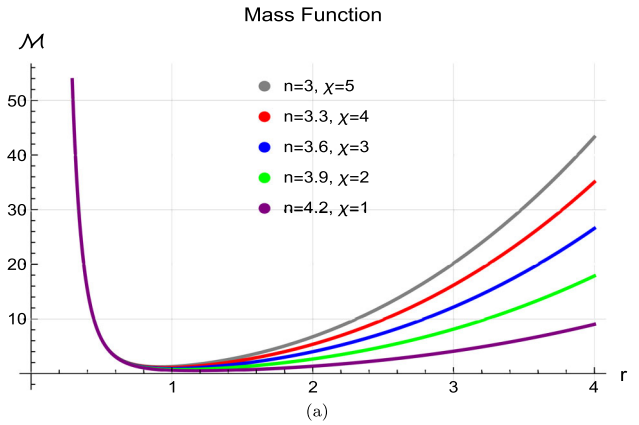

(a)

Fig. 2 Behavior of mass function $\mathcal{M}$ for the parametric values $r_0 = 0.5$, $k = 4$, $h = 2$, $\mu_0 = 0.1$, and selected values of Einasto parameter n and dimensionless parameter χ

tional sector, one provides a smooth and radially decreasing energy density that affects the entire gravitational behavior of the WH. Key to this is that energy conditions such as the null, weak, and dominant energy conditions, are being probed on the effective matter distribution, including contributions from both sectors. This decomposition makes it possible to identify where and how the requirements on exotic matter appear. The violations will be localized near the throat, while the exterior parts can meet all the classical energy conditions. Therefore, the MGD method not only elucidates the function of every component in the matter distribution but also allows for the creation of WHs with few and local violations, making the solutions more theoretically desirable and near physical reality. The expression for the effective matter variables is given as follows

$$\mu = \underbrace{\chi\mu_0 e^{-\left(\frac{r}{h}\right)^{1/n}}}_{\Theta_0^0} - \underbrace{\frac{(kr_0)\left(\frac{r_0}{r}\right)^k}{r^3}}_{\tilde{\mu}}, \tag{40}$$

$$\mathcal{P}_r = \underbrace{\frac{\chi h^3\mu_0 n}{r^3}\left\{\Gamma\left(3n,\left(\frac{r}{h}\right)^{1/n}\right) - \Gamma\left(3n,\left(\frac{r_0}{h}\right)^{1/n}\right)\right\}}_{\Theta_1^1} - \underbrace{\frac{r_0}{r^3}\left(\frac{r_0}{r}\right)^k}_{\tilde{\mathcal{P}}_r}, \tag{41}$$

$$\mathcal{P}_\dagger = -\underbrace{\frac{\chi\mu_0 e^{-\left(\frac{r}{h}\right)^{1/n}}}{2r^3}\left\{-h^3 n e^{\left(\frac{r}{h}\right)^{1/n}}\Gamma\left(3n,\left(\frac{r_0}{h}\right)^{1/n}\right) + h^3 n e^{\left(\frac{r}{h}\right)^{1/n}}\Gamma\left(3n,\left(\frac{r}{h}\right)^{1/n}\right) + r^3\right\}}_{\Theta_2^2} + \underbrace{\frac{(k+1)r_0}{2r^3}\left(\frac{r_0}{r}\right)^k}_{\tilde{\mathcal{P}}_\dagger}. \tag{42}$$

Figure 3 describes these matter variables graphically. In the decoupled WH solution obtained with the MGD method with the Einasto density profile, the analysis of energy conditions shows significant physical implications. The matter variables traced on plots, energy density μ, radial pressure $\mathcal{P}_r$, and tangential pressure $\mathcal{P}_\dagger$, display characteristic trends as functions of the Einasto index n. In our case, the effective energy density μ obtained under the MGD scheme with the Einasto density profile is strictly positive for $r > r_0$, as depicted in Fig. 3a. The tiny negative area lying extremely near the throat $r \approx r_0$ is a local consequence of the decoupling sector, which occurs quite naturally in anisotropic configurations in which exotic matter cannot be avoided in order to maintain the flare-out condition of a traversable WH [18,66]. Crucially, this negative contribution does not pervade the entire spacetime, but is restricted to a very thin neighborhood of the throat and rapidly gives way to positive values in accordance with the Einasto halo profile. Analogous localized violations have been encountered in other WH structures in modified gravity and MGD setups [27,32,41], where exoticity is reduced but not completely avoided. Therefore, the physical reasonableness of our WH solution relies on showing that exotic matter is limited and bounded by astrophysically motivated dark matter distributions, thus making the setup more realistic.

The presence of a negative tangential speed of sound in a certain region of the configuration does not reflect a genuine violation of hyperbolicity. In relativistic hydrodynamics, hyperbolicity guarantees the causality of the system of field equations and that perturbations propagate at real characteristic speeds [67]. In the current MGD formulation, even if the squared tangential sound speed $v_\dagger^2$ becomes negative, this is due to the anisotropic pressure response and not a consequence of a true breakdown in hyperbolicity. The effective tangential equation of state gets locally non-barotropic as a result of geometry deformation and dark matter coupling, producing an apparent negative gradient without entailing imaginary propagation velocities. Thus, the regions where $v_\dagger^2 < 0$ only indicate prevalence of anisotropic stresses characteristic of exotic matter instead of a failure of causal or hyperbolic structure. Such an interpretation establishes that the dynamical system on hand is still well-posed, causal, and

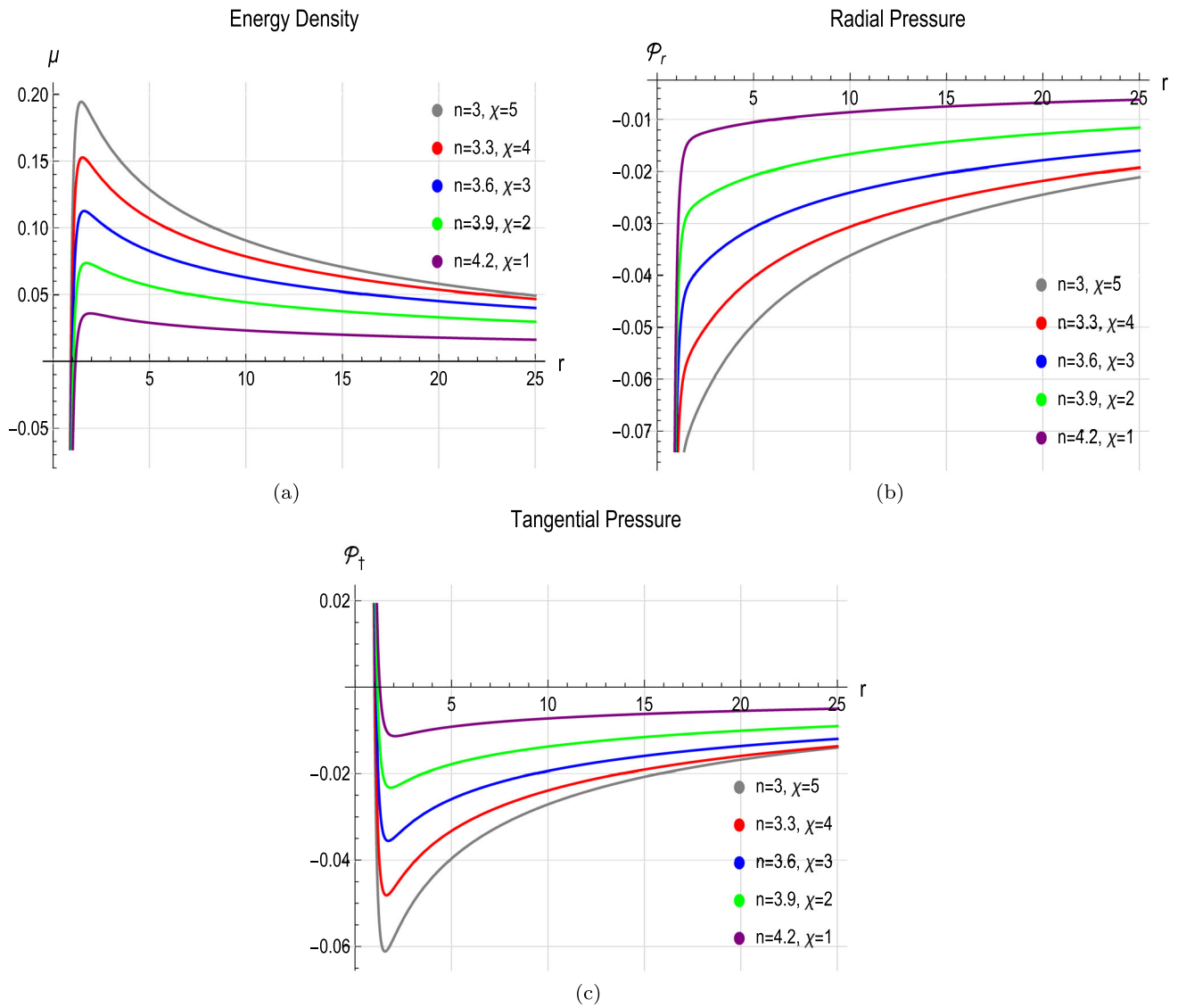

Fig. 3 Graphical analysis of modified matter variables for $r_0 = 0.5$, k = 4, h = 2, $\mu_0 = 0.1$, and selected values of Einasto index n and decoupling parameter χ

regular in the context of GR and the MGD scheme of decoupling.

In addition, both the radial pressure $\mathcal{P}_r$ and tangential pressure $\mathcal{P}_\dagger$ are negative across the whole spacetime, as needed to sustain the flaring-out condition of the geometry of the WH. The Null Energy Condition (NEC), which includes the combinations $\mu + \mathcal{P}_r$ and $\mu + \mathcal{P}_\dagger$, is also evidently violated near the throat because of the combined negativity of these quantities (as illustrated in Fig. 4). Nonetheless, for n to be increased, such violations become more and more localized and weaker at large r, meaning that higher values of the Einasto index correspond to configurations which become physically acceptable matter distributions at distances from the throat. This demonstrates the benefit of the MGD decoupling technique. Through proper selection of the profile parameters and anisotropic decomposition, it enables the generation of WHs with controlled energy condition violations and space-confining exotic matter.

The radial and tangential EoS parameters are defined and given by the following expressions

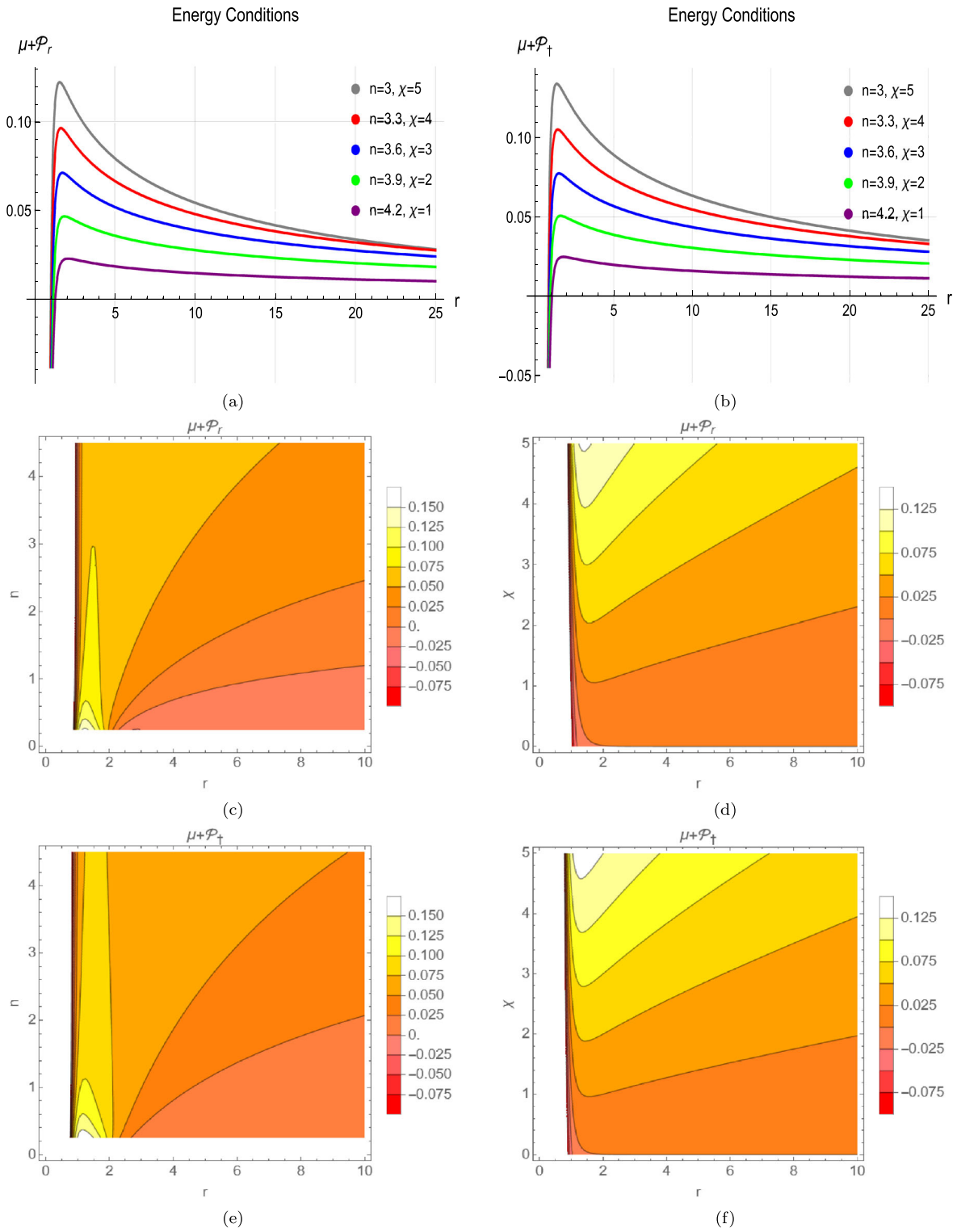

Fig. 4 Graphical depiction of NEC for the parametric values $r_0 = 0.5$, $k = 4$, $h = 2$, $\mu_0 = 0.1$, and differect Einasto index n and dimensionless parameter χ. In contour plots, $\chi = 3$ is kept fixed and the parameter n is allowed to vary and vice versa

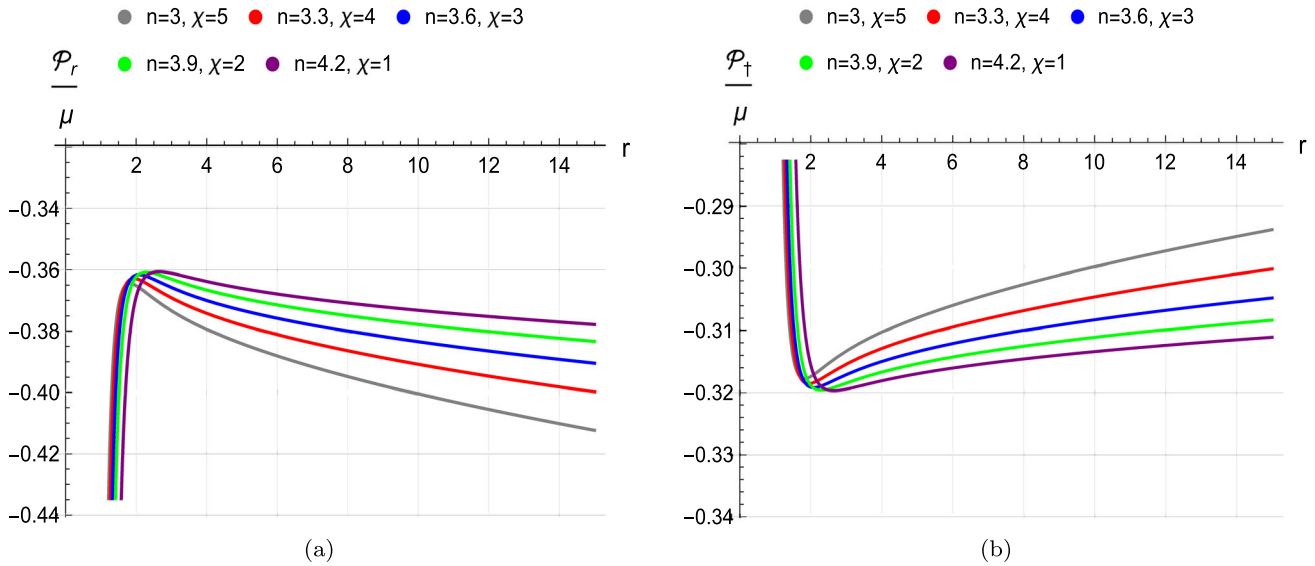

Fig. 5 Graphical depiction of EoS parameters for $r_0 = 0.5$, k = 4, h = 2, $\mu_0 = 0.1$, and different Einasto index n and dimensionless parameter χ

$$\mathcal{W}_r = \frac{\mathcal{P}_r}{\mu} = \frac{e^{\left(\frac{r}{h}\right)^{1/n}}\left\{-\chi h^3\mu_0 n\Gamma\left(3n,\left(\frac{r}{h}\right)^{1/n}\right)+\chi h^3\mu_0 n\Gamma\left(3n,\left(\frac{r_0}{h}\right)^{1/n}\right)+r_0\left(\frac{r_0}{r}\right)^k\right\}}{kr_0 e^{\left(\frac{r}{h}\right)^{1/n}}\left(\frac{r_0}{r}\right)^k-\chi\mu_0 r^3}, \tag{43}$$

$$\mathcal{W}_\dagger = \frac{\mathcal{P}_\dagger}{\mu} = \frac{\chi h^3\mu_0\left\{-n\Gamma\left(3n,\left(\frac{r_0}{h}\right)^{1/n}\right)+\frac{r^3}{h^3}e^{-\left(\frac{r}{h}\right)^{1/n}}+n\Gamma\left(3n,\left(\frac{r}{h}\right)^{1/n}\right)\right\}-(k+1)r_0\left(\frac{r_0}{r}\right)^k}{2kr_0\left(\frac{r_0}{r}\right)^k-2\chi r^3\mu_0 e^{-\left(\frac{r}{h}\right)^{1/n}}}. \tag{44}$$

The radial and tangential EoS parameters' behavior, presented in Fig. 5a, b, indicates the anisotropic nature of the WH's effective matter content when considered under the MGD-decoupling formalism. Both $\frac{\mathcal{P}_r}{\mu}$ and $\frac{\mathcal{P}_\dagger}{\mu}$ have negative values within the domain of consideration, which is consistent with the general requirement of having negative pressure (or tension) for supporting WH throats. In Fig. 5a, the radial EoS parameter $\mathcal{W}_r$ increases very steeply at first and afterwards goes down slowly with a growing r, exhibiting softer pressure gradient for larger n and smaller χ. This means that larger Einasto indices and smaller decoupling parameters decrease the effective radial tension. In contrast, Fig. 5b illustrates that the tangential EoS parameter $\mathcal{W}_\dagger$ has a sharp decay at a very small radial distance, followed by a linear increase with r, with higher n values resulting in more rapid stabilization. Remarkably, both EoS parameters exhibit convergence at large r, consistent with the anisotropic effects weakening far from the throat, and implying asymptotic matching to a more isotropic spacetime. These tendencies imply that adjusting n and χ can control the anisotropic stresses essential to ensure WH solutions are stable and traversable.

5 Exoticity parameter

Prior discussions demonstrate that the exotic matter distribution drives the minimally deformed Morris–Throne-WH solution. Compared to the pure GR case, it is clear that the Θ-sector, which is related to the dark energy or dark matter distribution, greatly reduces the magnitude of the energy condition violation. To ascertain whether the MGD components can effectively contribute exotic matter to stabilize the WH structure, the exoticity parameter $\mathfrak{X}$ may be utilized [18,56]. It is provided as

$$\mathfrak{X} = \frac{\mathcal{P}_r - \mu}{|\,\mu\,|}, \tag{45}$$

We can also define the exoticity parameter in terms of the shape function as

$$\mathfrak{X} = \frac{S - rS'}{r\,|\,S'\,|}. \tag{46}$$

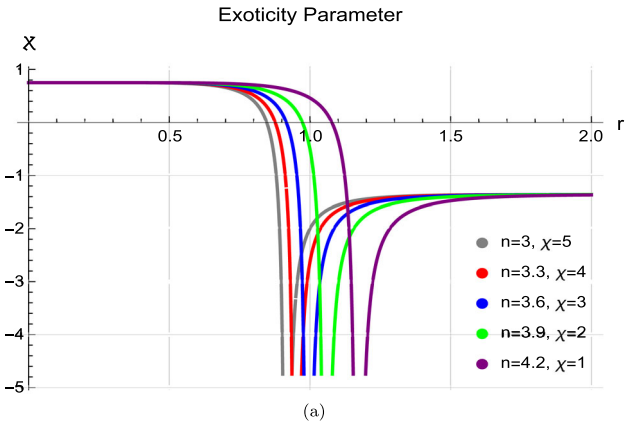

(a)

Fig. 6 The exoticity parameter is shown graphically for the parametric values $r_0 = 0.5$, $k = 4$, $h = 2$, and $\mu_0 = 0.1$, as well as different dimensionless parameter χ and Einasto index n

The exoticity parameter $\mathfrak{X}$ behavior is important in determining the places where exotic matter, with a negative energy density violating the NEC, is dominant. In the graph given in Fig. 6, $\mathfrak{X}$ drops sharply to negative values close to the WH throat, which is the feature signature of the presence of exotic matter. The sharpness and depth of the dip depend on the Einasto index n and the MGD decoupling parameter χ, which implies that exotic matter composition is responsive to both the density profile and the intensity of the geometric deformation. As r grows, the exoticity parameter approaches a negative constant asymptotically, which means that although the exotic effects will be reduced with radial distance, they can remain weakly present away from the throat. This is in accordance with the need for localized exotic matter around the throat to support a traversable WH, with the spacetime relaxing towards normal matter at bigger radii. Therefore, the analysis verifies that exoticity is localized around the throat and can be tuned by adjusting n and χ.

6 Spacetime singularity

The inevitable occurrence of spacetime singularities in physically relevant solutions of the GR field equation is one of the most well-known and persistent problems in GR [68]. Densities and curvature invariants grow infinitely and diverge at a singularity, which is a spacetime event. Such an event has considerable consequences for topics like physical determinism, causality, predictability, and the applicability of the conventional laws of physics. It is generally accepted that spacetime singularities are problematic because the classical framework of GR is not predictive and, as a result, is no longer useful when basic quantities increase to infinity. Therefore, the emergence of a spacetime singularity indicates that the theory has been used outside of its scope [69]. Quasi-regular, non-scalar curvature, and scalar curvature singularities are the three main categories into which the fundamental singularities of a spacetime can be divided. The conical singularity in the cosmic string's spacetime serves as an illustration of the first one [70]. Singularities whose curvature scalars do not behave badly are the second category [71]. If there is an issue with a component of the Ricci tensor, these singularities are also known as matter singularities. Curvature invariants like Kretschmann scalar diverge on at least one causal curve, and scalar curvature singularities are the endpoint of that curve. One can cite the inner Schwarzschild solution and the universe's initial singularity as instances of these kinds of singularities; for further information, [72]. It is widely acknowledged that the presence of a spacetime singularity is strongly indicated by the geodesic incompleteness and the divergence of the curvature invariants [73]. One could argue that the issue of spacetime singularities is significant in WH physics in light of these factors. The abnormal behavior of extreme regions (such as the failure of physical laws) at the vicinity of the singularity can be transferred from one universe to the other if the singularity is present in the spacetime of one of the universes connected by the WH. Alternatively, if the throat is singular, these effects may be transferred to both Universes connected by the WH throat. This may occur in the event of a timelike singularity, such as at the throat, to which a test particle may approach arbitrarily before departing the singular region. If this is the case, the test particle might disrupt the established laws of physics in other universes and bring the basic issues listed above with it [74].

The MGD method deforms the geometry smoothly, when applied to an Einasto dark matter halo. The resulting configuration maintains a consistent causal structure and features finite curvature. Such behaviors have also been recently observed for MGD and dark matter-inspired WH geometries, which also possess curvature-regular interiors and finite tidal forces [75–81]. The results conform to the overall trend in recent literature favoring singularity prevention through gravitational decoupling and dark-energy like corrections [75,82]. These solutions have a regular and well-behaved geometrical structure all along the spacetime. Within the context of the Hawking–Penrose singularity theorems [83], the appearance of singularities in GR depends on the simultaneous satisfaction of three primary conditions: (i) the strong energy condition (SEC) being valid, (ii) the lack of causality violations, and (iii) the presence of trapped surfaces. In the current MGD setup, these assumptions are relaxed or are no longer valid, resulting in singularity-free WH configurations [84]. The evolutions of $\mu + \mathcal{P}_r$ and $\mu + \mathcal{P}_\dagger$ in Fig. 3 tell us that the NEC is violated slightly in a small region near the throat but is positive elsewhere. This localized violation is enough to support the WH geometry without causing curvature singularities. Since the Hawking–Penrose singularity theorems depend on global convergence conditions com-

bined with trapped surfaces, those localized NEC violations inherently forbid geodesic incompleteness to occur. Consequently, the absence of curvature divergences and the regular profiles of μ and $\mathcal{P}_i$ imply that our solutions are regular and evade classical singularities in the sense of the theorems.

Therefore, we need the spacetime singularities to be absent at the throat and throughout the spacetime for a physically plausible WH configuration. In order to achieve this, we calculate the Kretschmann invariant, which for the line element (2) has the following structure.

$$\begin{aligned}\mathbb{K} &= \mathfrak{R}^{abcd}\mathfrak{R}_{abcd} \\ &= \frac{1}{r^6}\left\{4r^3(r-S)\left(R'\right)^3\left(S-rS'\right)+8r^3(r-S)R'R''\right. \\ &\quad \left(-\frac{1}{2}rS'+r(r-S)R'+\frac{S}{2}\right) \\ &\quad +r^2R'^2\left(r^2\left(S'\right)^2-2rSS'-16rS+9S^2+8r^2\right) \\ &\quad \left.+2r^2S'^2-4rSS'+4r^4(r-S)^2\left(R''^2+R'^4\right)+6S^2\right\}. \end{aligned} \tag{47}$$

Since all of the EMT components are finite in the limit of approach to the throat, we first observe that the matter distribution behaves regularly at the throat, i.e., a singularity-free EMT. The Kretschmann scalar is found as

$$\begin{aligned}\mathbb{K} &= \frac{1}{r^6}\left\{2\left(kr_0\left(\frac{r_0}{r}\right)^k-\chi r^3\mu_0 e^{-\left(\frac{r}{h}\right)^{1/n}}\right)^2\right. \\ &\quad +6\left(\chi h^3\mu_0 n\left[\Gamma\left(3n,\left(\frac{r_0}{h}\right)^{1/n}\right)-\Gamma\left(3n,\left(\frac{r}{h}\right)^{1/n}\right)\right]\right. \\ &\quad \left.+r_0\left(\frac{r_0}{r}\right)^k\right)^2-4\left(\chi r^3\mu_0 e^{-\left(\frac{r}{h}\right)^{1/n}}-kr_0\left(\frac{r_0}{r}\right)^k\right) \\ &\quad \left[\chi h^3\mu_0 n\left(\Gamma\left(3n,\left(\frac{r_0}{h}\right)^{1/n}\right)-\Gamma\left(3n,\left(\frac{r}{h}\right)^{1/n}\right)\right)\right. \\ &\quad \left.\left.+r_0\left(\frac{r_0}{r}\right)^k\right]\right\}. \end{aligned} \tag{48}$$

The aforementioned amounts at the throat will manifest as

$$\begin{aligned}\mathbb{K}|_{r=r_0} &= \frac{1}{r_0^6}\left\{-4(k+1)\mu_0 r_0^4\chi e^{-\left(\frac{r_0}{h}\right)^{1/n}}\right. \\ &\quad \left.+2\mu_0^2 r_0^6\chi^2 e^{-2\left(\frac{r_0}{h}\right)^{1/n}}+2\left(k^2+2k+3\right)r_0^2\right\}. \end{aligned} \tag{49}$$

We can infer from the above expressions that for these WH solutions, the Kretschmann invariant is finite at the throat. Additionally, this quantity behaves consistently at the WH throat for $r_0 = 0.5$, $k = 4$, $h = 2$, $\mu_0 = 0.1$ and positive values of χ and Einasto index n (as shown in Fig. 7). Consequently, the throat does not have a curvature singularity. We also observe that these quantities asymptotically tend to zero and behave well for $r > r_0$. Therefore, there isn't a curvature singularity in the WH spacetime.

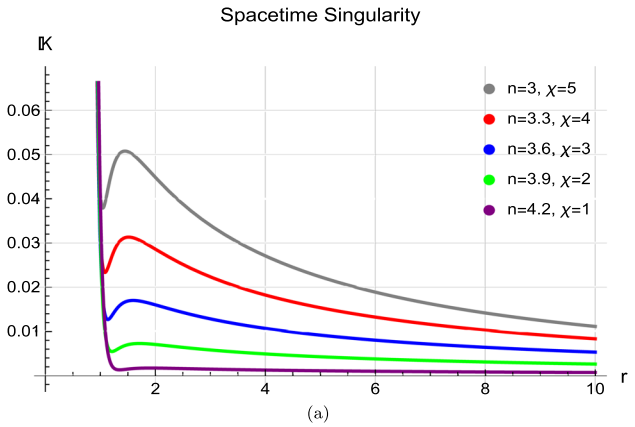

Fig. 7 Graphical behaviour of spacetime singularity for specific parametric values

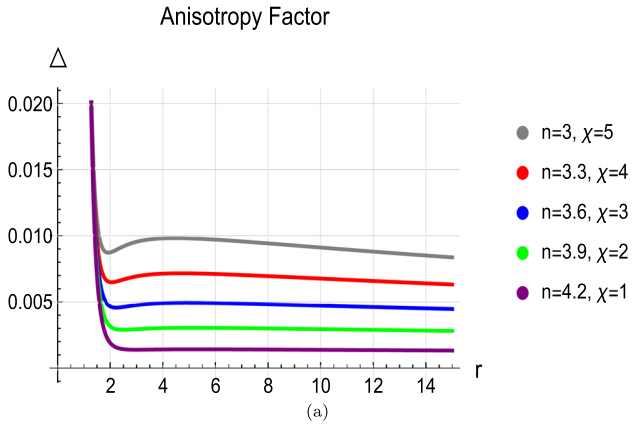

Fig. 8 Anisotropy factor for fixed values of some parameters as $r_0 = 0.5$, $k = 4$, $h = 2$, $\mu_0 = 0.1$, and varying n and χ

7 Stability assessment tests

7.1 Anisotropy and pressure gradient

In the context of MGD framework, anisotropy is naturally generated by the geometric term Θ^{η}_{β} independent of the usual matter sector. For WH solutions built within the Einasto density profile, a well-established dark matter halo model, we calculated the anisotropy parameter $\triangle = \mathcal{P}_{\dagger} - \mathcal{P}_r$ to study the pressure distribution along various directions. Our results show that $\triangle > 0$ (as shown in Fig. 8) in the entire radial range, meaning that the tangential pressure is greater than the radial pressure. This positive anisotropy creates a repulsive force outward that is crucial to balance the gravitational pull and maintain the WH structure. This action is particularly significant closer to the throat, where the structure is under

greatest threat from gravitational collapse. The existence of a positive anisotropic force not only confirms the flaring out condition but also makes a considerable contribution to the fulfillment of the static equilibrium conditions of the generalized Tolman–Oppenheimer–Volkoff (TOV) equation.

In the MGD formalism, the anisotropy effectively changes the internal pressure gradients, thus improving the stability of the structure without recourse to exotic matter in the usual sense. Such a behavior is consistent with the overall physical expectation for anisotropic self-gravitating systems, in which $\triangle > 0$ is recognized to enhance stability margins [85]. As a result, the anisotropy generated through MGD, together with an empirical dark matter profile such as the Einasto distribution,n not only maintains the geometry of the WH but also supports its physical acceptability and static stability.

7.2 Cracking and casuality

In WH configurations, especially in those sustained by anisotropic matter through the MGD decoupling, the determination of cracking and causality conditions is crucial for the stability analysis of the solution. Cracking arises when the radial and tangential sound speeds become so large that they diverge, which in turn may cause internal instability in the structure. Such a behavior is diagnosed through inspection of the sign and size of the quantity ${v_\dagger}^2 - {v_r}^2$, where a sign change can signal the existence of a cracking point in the matter distribution. Second, the causality condition demands that radial and tangential sound speeds are subluminal, i.e., in the interval [0, 1]. For MGD WHs with Einasto density profile, these analyses are important indicators of the physical acceptability of the model. Regions where both sound speeds fulfill causality and $\mid {v_\dagger}^2 - {v_r}^2 \mid < 1$ are read as causally stable and crack-free. Therefore, checking these conditions throughout the WH geometry guarantees that the effective matter distribution not just sustains the exotic topology but does so without compromising basic physical principles [86]. The following are the expressions for the radial and tangential sound speeds.

$$v_r^2 = \frac{d\mathcal{P}_r}{d\mu}, \quad v_\dagger^2 = \frac{d\mathcal{P}_\dagger}{d\mu}. \tag{50}$$

The sound speed analysis in the WH configuration provides important information about its physical stability and the nature of the stabilizing matter. In the current model, the radial sound speed falls in the physically acceptable interval $0 < v_r^2 < 1$, meeting the causality condition and signaling that the radial perturbations propagate subluminally. But the tangential speed of sound is found to be negative. The occurrence of a negative tangential sound speed $v_\dagger^2$ close to the WH throat in Fig. 9b is not to be considered unphysical, but as an expression of the anisotropic pressures needed to maintain exotic geometries. It is well known that traversable WHs are necessarily involve matter sources that violate standard energy conditions [18,66,87]. In our scenario, the MGD decoupling combined with the Einasto density profile creates very strong local anisotropies, which can temporarily force $v_\dagger^2$ negative in the throat neighborhood. This characteristic does not destabilize physically, as the radial sound speed remains causal ($0 \leq v_r^2 \leq 1$) and the cracking condition $\mid v_\dagger^2 - v_r^2 \mid < 1$ is fulfilled throughout the configuration [86,88]. Comparable anisotropic deviations have been talked about in recent works on WHs in dark matter halos and modified gravity settings, where stability remains intact in the face of local exotic effects [24,89]. Thus, the negative v_t^2 must be viewed as a signal of the exotic anisotropy necessary to sustain the MGD-Einasto WH configurations, in full accordance with contemporary theory of traversable WH physics.

7.3 Conservation equation

Within the context of MGD-decoupling, conservation of the total effective EM tensor implies a generalized equilibrium condition. This is formulated through the vanishing of the covariant divergence of the effective tensor,$\nabla_\beta T_\eta^\beta$, and results in a TOV-like equation for anisotropic and decoupled matter content. In the case of anisotropies and the extra gravitational source injected through the decoupling, the conservation equation has the form

$$\frac{d\mathcal{P}_r}{dr} - \frac{2}{r}\left(\mathcal{P}_\dagger - \mathcal{P}_r\right) = 0. \tag{51}$$

This equation regulates the force balance within the system of the WH and emphasizes the contributions of gravitational attraction, hydrostatic pressure, and anisotropic stresses. The term having R is missing, as we have taken into account $R = 0$. Nevertheless, the missing term can be recovered, and a gravitational gradient (associated with tidal force) is introduced into the system when the red-shift function is not assumed to be constant. The introduction of the decoupling term makes it possible to describe exotic matter and geometric deformations, required to maintain traversable wormhole solutions. The equilibrium condition is given by $F_A + F_H = 0$, where the hydrostatic and anisotropic forces, F_H and F_A are defined as

$$F_H = -\frac{d\mathcal{P}_r}{dr}, \quad F_A = -\frac{2}{r}\left(\mathcal{P}_\dagger - \mathcal{P}_r\right). \tag{52}$$

Figure 10 shows the behavior of these forces and ensures that these forces cancel the effect of each other completely. This kind of behavior indicates the achievement of an equilibrium state and ensure the existence of viable WH configurations.

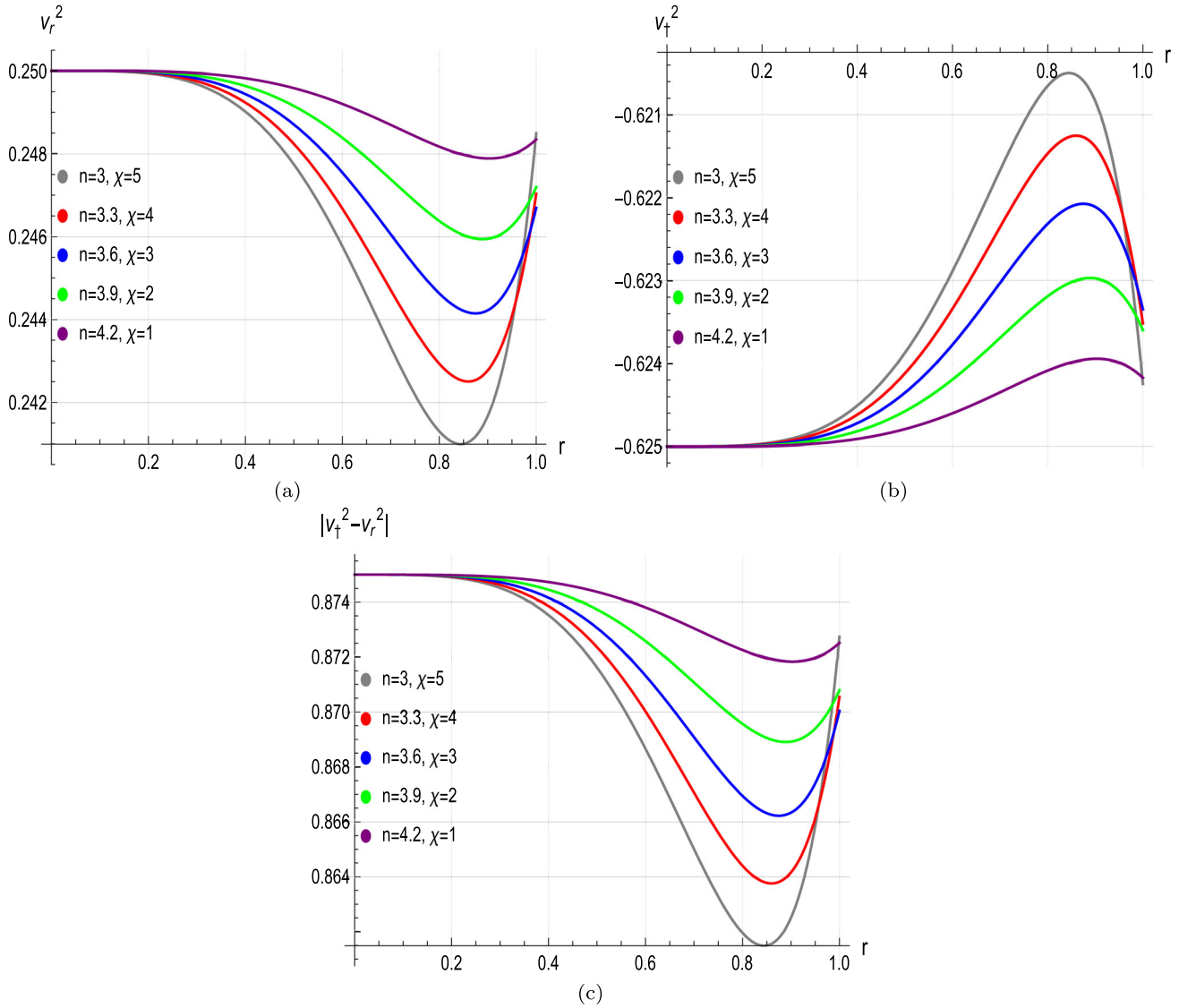

Fig. 9 Cracking and casuality analysis for specific parametric values as $r_0 = 0.5$, $k = 4$, $h = 2$, $\mu_0 = 0.1$, and different Einasto index n and dimensionless parameter χ

7.4 Complexity of the configurations

The theoretical framework of relativistic complexity in self-gravitating systems has been considerably refined in recent years, especially through the seminal work of Herrera and coworkers. The first generalization was in the case of dynamical, spherically symmetric dissipative systems, where Herrera [90] provided a formalism for computing the structure of evolving fluids outside equilibrium. This framework was extended to investigate the complexity of self-gravitating systems by Herrera [91], where a general overview associated complexity with inhomogeneity and anisotropy of matter content. A further insight was gained in [92], where a new definition of complexity for static, spherically symmetric solutions was proposed. In this context, the scalar function Y_{th}, extracted from the orthogonal decomposition of the Riemann tensor, was suggested as a natural measure of complexity. This scalar compresses both pressure anisotropy and density inhomogeneity, and is zero when absent from both, establishing a strong test for simplicity of structure.

The complexity idea was also generalized to more general geometries by Herrera. In [93], the Bondi metric was examined in order to establish complexity in radiative spacetimes, whereas in [93] the formalism was applied to axially symmetric static sources, giving further applicability within astrophysical modeling. Lastly, stability of conditions such as isotropic pressure was also explored in [94], where the interplay between equilibrium and complexity allowed for the determination of structurally stable configurations. These are directly applicable to the WH geometries in the MGD-

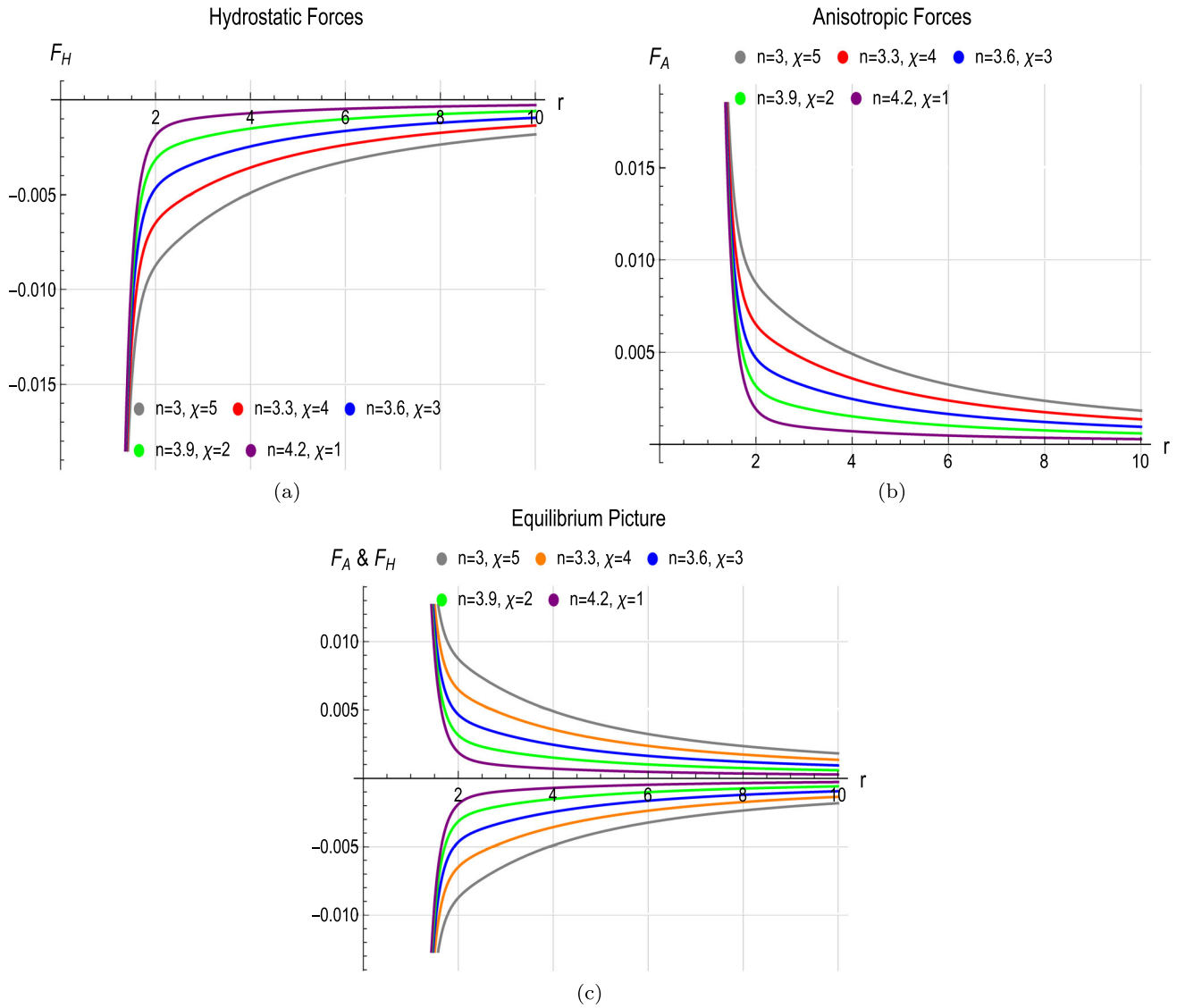

Fig. 10 Equilibrium analysis for specific parametric values as $r_0 = 0.5$, k = 4, h = 2, $\mu_0 = 0.1$, and different Einasto index n and parameter χ

decoupled scheme, where anisotropies as well as matter distribution are essential, and where the factor of complexity serves to differentiate physically acceptable and stable models from unphysical ones.

$$\mathcal{Y}_{\mathcal{TF}} = (\mathcal{P}_r - \mathcal{P}_\dagger) - \frac{\int_{r_0}^{r} r^3 \frac{\partial \mu(z)}{\partial z}\, dz}{2z^3}. \tag{53}$$

The complexity factor's graphical plot (shown in Fig. 11) indicates that it varies between negative values and asymptotically approaches zero at greater radial distances. Physically, this feature is very important. The negative values of complexity near the WH throat reveal the anisotropic stresses and inhomogeneities that characterize the effective matter distribution at smaller radii. However, with a growing radial coordinate, the decreasing trend towards zero is a sign of a

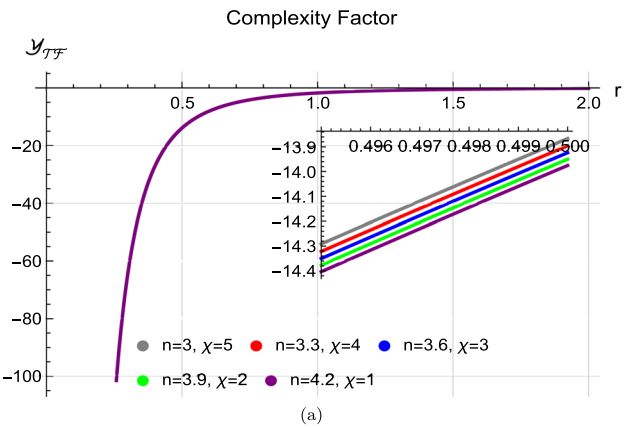

Fig. 11 Complexity factor analysis for $r_0 = 0.5$, $k = 4$, $h = 2$, and $\mu_0 = 0.1$, with different dimensionless parameter χ and Einasto index n

structured decrease in structural abnormalities. Convergence towards zero means that the system approaches a condition of minimal complexity characterized by decreasing pressure anisotropy and density gradients, a transition toward a stabler, less weird configuration of matter from the WH throat. This concurs with physically realistic geometries of the WH expectations, which consist of exotic matter concentrated in the throat and standard energy conditions asymptotically regained.

8 Conclusion

In this paper, we have investigated how gravitational decoupling influences WH spacetime, specifically the popular MT WH model, by means of an MGD method. We have sought the decoupler function $H(r)$ and the Θ-sector by using the time component of the Θ^{η}_{β} field to mimic the generalized Einasto dark matter density profile. A standard first-order differential equation in $H(r)$ can be solved by this choice (see Eqs. (24)–(28)). The equation system (17)–(19) is determined completely from the expression of the deformation function. Therefore, the seed WH spacetime given by (23) is also employed to derive the minimally extended shape function $S(r)$ and the effective thermodynamic parameters (9)–(11). The new region represented by the pair $\{\Theta^{\eta}_{\beta}, H(r)\}$ must satisfy some conditions in order to maintain the WH structure, since the seed solution itself fulfills all the constraints given in Sec. 1. In this context, the decoupling function $H(r)$ must vanish at the throat r_0 of the WH, i.e., $H(r_0) = 0$. This is due to the fact that r_0 is a value obtained by evaluating the seed shape function $\tilde{S}$ at the WH throat. In addition, satisfying the so-called flaring out condition at the throat of the WH is among the conditions for being a traversable WH topology between two regions. The dimensionless coupling parameter χ introduced by MGD has then been restricted in this instance to meet the flaring out condition (see Eq. (38)). It is well known that a WH in the world of GR cannot at the same time fulfill the flaring out requirement and all energy conditions, and this case is no exception. In this case, however, the MGD approach could be considered as an exotic matter regulator. Of course, the exotic matter is a required ingredient to stabilize the WH structure, but sometimes it is desirable to control the distribution of this exotic matter to have a small breaching of the energy conditions at the throat of the WH and around it. The minimally extended shape function $S(r)$ satisfies all the necessary criterion to describe the WH geometry as shown in Fig. 1. Furthermore NEC violation near WH throat is indicated in the plots of Figs. 3 and 4.

The EoS parameters exhibit convergence at large r, consistent with the anisotropic effects weakening far from the throat, and implying asymptotic matching to a more isotropic spacetime. These tendencies imply that adjusting n and χ can control the anisotropic stresses essential to ensure WH solutions are stable and traversable (see Fig. 5). The exoticity parameter behavior $\mathfrak{X}(r)$ (as shown in Fig. 6) implies that it is positive prior to the throat, showing that it satisfies the NEC, and turns negative shortly after the throat, indicating localized NEC violation required for traversability. This implies that exotic matter is localized around the throat, and the range can be regulated by adjusting parameters such as the Einasto index n and the deformation parameter χ. This kind of behavior improves the physical acceptability of dark matter-supported MGD WH. Figure 7 shows that these WH solutions are singularity-free.

A range of diagnostic methods was employed to examine the stability and physical viability of the MGD WH solutions. The outward-directed anisotropic force that helps in sustaining the throat geometry is established by the anisotropy factor (Fig. 8). The TOV equation is fully satisfied as shown in Fig. 9, ensuring the balance between anisotropic and hydrostatic forces. The causality condition were partially satisfied, while the radial sound speed remained within normal bounds, the tangential sound speed was discovered to be negative and the absolute difference $\mid {v_{\dagger}}^2 - {v_r}^2 \mid$ is still less than one, which mathematically meets the cracking condition (see Fig. 10). This kind of behavior usually implies the existence of exotic matter components or extremely anisotropic stress–energy distributions at the WH throat. The $v^2_{\dagger}$ negativity indicates a significant anisotropy of the extra-matter sector brought in through the MGD decoupling. However, the complexity factor converges to zero, signifying evolution towards geometric simplicity at very large radial distances (Fig. 11).

Interestingly, based on the results presented here, we may conclude that well-posed WH solutions threaded by a tiny amount of exotic matter dispersion can be constructed inside the context of GR using the gravitational decoupling by MGD approach. Additionally, the dimensionless coupling constant χ can be restricted to control the violation of the energy conditions at the WH throat. More importantly, a careful choice of α helps to maintain a positive defined density everywhere and permits the satisfaction of the energy conditions away from the WH throat. The imposition of deformation on the time component to bring in a non-vanishing red-shift function and the examination of the stability of the solutions to radial perturbations as large quantities of mass are injected via the structure are important aspects to note. Future studies will address these challenges.

Funding This paper receives no funding.

Data Availability Statement This manuscript has no associated data or the data will not be deposited. [Authors' Comment: Data sharing not applicable to this article as no datasets were generated or analysed during the current study.].

Code Availability Statement This manuscript has no associated code/software. [Authors' comment: Code/Software sharing not applicable to this article as no code/software was generated or analysed during the current study.].

Declarations

Conflict of interest The authors have no conflict of interest with respect to the publication of the present paper.

Funded by SCOAP[3].

References

1. R.M. Wald, *General Relativity* (University of Chicago Press, Chicago, 2010)
2. A. Einstein, N. Rosen, Phys. Rev. **48**, 73 (1935)
3. J.R. Oppenheimer, H. Snyder, Phys. Rev. **56**, 455 (1939)
4. M.D. Kruskal, Phys. Rev. **119**, 1743 (1960)
5. R.P. Kerr, Phys. Rev. Lett. **11**, 237 (1963)
6. T. Regge, J.A. Wheeler, Phys. Rev. **108**, 1063 (1957)
7. R. Penrose, Phys. Rev. Lett. **14**, 57 (1965)
8. A. Raychaudhuri, Phys. Rev. **98**, 1123 (1955)
9. D.-C. Dai, D. Stojkovic, Phys. Rev. D **100**, 083513 (2019)
10. L. Flamm, *Beiträge zur Einsteinschen gravitationstheorie* (Hirzel, 1916)
11. D.-C. Dai, D. Minic, D. Stojkovic, Eur. Phys. J. C **80**, 1 (2020)
12. D.-C. Dai, D. Minic, D. Stojkovic, Phys. Rev. D **98**, 124026 (2018)
13. J.A. Wheeler, Phys. Rev. **97**, 511 (1955)
14. H.G. Ellis, J. Math. Phys. **14**, 104 (1973)
15. V. De Falco, Phys. Rev. D **108**, 024051 (2023)
16. V. De Falco, M. De Laurentis, S. Capozziello, Phys. Rev. D **104**, 024053 (2021)
17. M.Y. Khlopov, B. Malomed, Y.B. Zeldovich, Mon. Not. R. Astron. Soc. **215**, 575 (1985)
18. M.S. Morris, K.S. Thorne, Am. J. Phys. **56**, 395 (1988)
19. Z. Yousaf, A. Adeel, M. Rizwan, G. Mustafa, A. Ali, Int. J. Geom. Methods Mod. Phys. **22**, 2550093 (2025)
20. V. De Falco, E. Battista, S. Capozziello, M. De Laurentis, Phys. Rev. D **101**, 104037 (2020)
21. V. De Falco, E. Battista, S. Capozziello, M. De Laurentis, Phys. Rev. D **103**, 044007 (2021)
22. E. Di Grezia, E. Battista, M. Manfredonia, G. Miele, Eur. Phys. J. Plus **132**, 1 (2017)
23. T. Naseer, M. Sharif, A. Fatima, S. Manzoor, Chin. J. Phys. **86**, 350 (2023)
24. T. Naseer, M. Sharif, M. Faiza, B. Dayanandan, Eur. Phys. J. C **84**, 1187 (2024)
25. A. Malik, T. Naz, A. Qadeer, M.F. Shamir, Z. Yousaf, Eur. Phys. J. C **83**, 522 (2023)
26. A.A. Filho, J. Reis, A. Övgün, Eur. Phys. J. C **85**, 83 (2025)
27. P. Channuie, Allah Ditta, N. Kaewkhao, A. Ovgun, Phys. Dark Universe **48**, 101963 (2025)
28. K. Jusufi, A. Övgün, Phys. Rev. D **97**, 024042 (2018)
29. W. Javed, R. Babar, A. Övgün, Phys. Rev. D **99**, 084012 (2019)
30. W. Javed, S. Riaz, R.C. Pantig, A. Övgün, Eur. Phys. J. C **82**, 1057 (2022)
31. M. Halilsoy, A. Ovgun, S.H. Mazharimousavi, Eur. Phys. J. C **74**, 1 (2014)
32. G. Mustafa, M. Ahmad, A. Övgün, M. Farasat Shamir, I. Hussain, Fortschr. Phys. **69**, 2100048 (2021)
33. J. Rayimbaev, U. Eshimbetov, B. Majeed, A. Abdujabbarov, A. Abduvokhidov, B. Abdulazizov, A. Xalmirzayev, Chin. Phys. C **48**, 055104 (2024)
34. O. Rahimov, B. Toshmatov, Y. Vyblyi, A. Akhmedov, B. Abdulazizov, Phys. Dark Univ. **44**, 101483 (2024)
35. B. Toshmatov, K. Mavlyanov, B. Abdulazizov, A. Mamadjanov, F. Atamurotov, Ann. Phys. **458**, 169450 (2023)
36. S. Mardonov, J. Rayimbaev, F. Abdulkhamidov, E. Karimbaev, B. Abdulazizov, Class. Quantum Gravity **42**, 115004 (2025)
37. R. Casadio, J. Ovalle, R. Da Rocha, Class. Quantum Gravity **31**, 045016 (2014)
38. R. Casadio, J. Ovalle, R. Da Rocha, Europhys. Lett. **110**, 40003 (2015)
39. R. Casadio, J. Ovalle, R. Da Rocha, Class. Quantum Gravity **32**, 215020 (2015)
40. J. Ovalle, R. Casadio, R. Da Rocha, A. Sotomayor, Eur. Phys. J. C **78**, 122 (2018)
41. J. Ovalle, Phys. Rev. D **95**, 104019 (2017)
42. L. Gabbanelli, Á. Rincón, C. Rubio, Eur. Phys. J. C **78**, 370 (2018)
43. C. Las Heras, P. León, Fortschr. Phys. **66**, 1800036 (2018)
44. J. Ovalle, A. Sotomayor, Eur. Phys. J. Plus **133**, 428 (2018)
45. R. Casadio, E. Contreras, J. Ovalle, A. Sotomayor, Z. Stuchlik, Eur. Phys. J. C **79**, 826 (2019)
46. J. Ovalle, R. Casadio, Rd. Rocha, A. Sotomayor, Z. Stuchlík, Eur. Phys. J. C **78**, 960 (2018)
47. G. Panotopoulos, Á. Rincón, Eur. Phys. J. C **78**, 851 (2018)
48. J. Ovalle, Phys. Lett. B **788**, 213 (2019)
49. J. Einasto, Astron. Nachr. **291**, 97 (1969)
50. S. Sushkov, Phys. Rev. D **71**, 043520 (2005)
51. Z. Yousaf, K. Bamba, B. Almutairi, M. Bhatti, M. Rizwan, Nucl. Phys. B **1018**, 116997 (2025)
52. Z. Yousaf, B. Almutairi, M. Rizwan, T. Ganesan, M. Bhatti, Int. J. Mod. Phys. D **34**, 2450072 (2025)
53. M. Cataldo, F. Orellana, Phys. Rev. D **96**, 064022 (2017)
54. Z. Xu, M. Tang, G. Cao, S.-N. Zhang, Eur. Phys. J. C **80**, 70 (2020)
55. F. Tello-Ortiz, S.K. Maurya, P. Bargueño, Eur. Phys. J. C **81**, 426 (2021)
56. M.S. Morris, K.S. Thorne, U. Yurtsever, Phys. Rev. Lett. **61**, 1446 (1988)
57. D. Hochberg, M. Visser, Phys. Rev. Lett. **81**, 746 (1998)
58. D. Hochberg, M. Visser, Phys. Rev. D **56**, 4745 (1997)
59. L. Gao, J.F. Navarro, S. Cole, C.S. Frenk, S.D. White, V. Springel, A. Jenkins, A.F. Neto, Mon. Not. R. Astron. Soc. **387**, 536 (2008)
60. R.P. Graterol, Eur. Phys. J. Plus **133**, 244 (2018)
61. R. Dehghani, P. Salucci, H. Ghaffarnejad, Astron. Astrophys. **643**, A161 (2020)
62. S. Khan, J. Rayimbaev, I. Ibragimov, S. Muminov, A. Dauletov, Ann. Phys. **481**, 170130 (2025)
63. S.A. Cellone, J.C. Forte, D. Geisler, Astrophys. J. **93**, 397 (1994)
64. N. Caon, M. Capaccioli, M. D'Onofrio, Mon. Not. R. Astron. Soc. **265**, 1013 (1993)
65. Y. Andredakis, R. Peletier, M. Balcells, Mon. Not. R. Astron. Soc. **275**, 874 (1995)

66. M. Visser, Woodbury (1995)
67. Z. Hassan, A. Bhat, P.K. Sahoo, Eur. Phys. J. C **85**, 930 (2025)
68. S.W. Hawking, G.F. Ellis, *The Large Scale Structure of Space-Time* (Cambridge University Press, Cambridge, 2023)
69. A.D. Rendall, in *100 Years of Relativity: Space-time Structure: Einstein and Beyond*. (World Scientific, Singapore, 2005), p.76
70. J.M. Senovilla, Gen. Relativ. Gravit. **30**, 701 (1998)
71. G.F. Ellis, B.G. Schmidt, Gen. Relativ. Gravit. **8**, 915 (1977)
72. C.B. Collins, G.F.R. Ellis, Phys. Rep. **56**, 65 (1979)
73. P.S. Joshi, *Gravitational Collapse and Spacetime Singularities* (Cambridge University Press, Cambridge, 2007)
74. J. Earman, Found. Phys. **26**, 623 (1996)
75. P. Panyasiripan, N. Kaewkhao, P. Channuie, A. Övgün, Nucl. Phys. B **1004**, 116563 (2024)
76. F. Tello-Ortiz, B. Mishra, A. Alvarez, K.N. Singh, Fortschr. Phys. **71**, 2200108 (2023)
77. M. Yousaf, A. Rehman, M.M.M. Nasir, S. Hanif, H. Asad, Commun. Theor. Phys. (2025). https://doi.org/10.1088/1572-9494/ae015a/meta
78. Z. Yousaf, M. Rizwan, M. Alshammari, O.A. Almatroud, S. Alshammari, M.M. Al-sawalha, Eur. Phys. J. C **85**, 1 (2025)
79. Z. Yousaf, M.Z. Bhatti, M. Rizwan, J. Rayimbaev, I. Ibragimov, I. Davletov, Nucl. Phys. B **1019**, 117128 (2025)
80. Z. Yousaf, M. Rizwan, M. Alshammari, O.A. Almatroud, S. Alshammari, M.M. Al-sawalha, Phys. Dark Univ. **50**, 102082 (2025)
81. M. Alshammari, M. Rizwan, O.A. Almatroud, S. Alshammari, Z. Yousaf, Int. J. Geom. Methods Mod. Phys. (2025). https://doi.org/10.1142/S021988782650009X
82. S. Chaudhary, S.K. Maurya, J. Kumar, Chin. J. Phys. **97**, 1036 (2025)
83. S.W. Hawking, R. Penrose, Proc. R. Soc. Lond. A **314**, 529 (1970)
84. J.M. Senovilla, D. Garfinkle, Class. Quantum Gravity **32**, 124008 (2015)
85. L. Herrera, N.O. Santos, Phys. Rep. **286**, 53 (1997)
86. H. Abreu, H. Hernández, L.A. Núnez, Class. Quantum Gravity **24**, 4631 (2007)
87. F.S. Lobo, *Wormholes, Warp Drives and Energy Conditions*, vol. 189 (Springer, Berlin, 2017)
88. L. Herrera, Phys. Lett. A **165**, 206 (1992)
89. F. Rahaman, B. Samanta, N. Sarkar, B. Raychaudhuri, B. Sen, Eur. Phys. J. C **83**, 395 (2023)
90. L. Herrera, Phys. Rev. D **97**, 044010 (2018)
91. L. Herrera, Entropy (Basel) **23**, 802 (2021)
92. L. Herrera, A. Di Prisco, J. Ospino, Phys. Rev. D **98**, 104059 (2018)
93. L. Herrera, A. Di Prisco, J. Carot, Phys. Rev. D **99**, 124028 (2019)
94. L. Herrera, Phys. Rev. D **101**, 104024 (2020)